International Forum on Aeroelasticity and Structural Dynamics
IFASD 2022
13-17 June 2022, Madrid, Spain

ACTIVE FLUTTER SUPPRESSION OF A TWO-DIMENSIONAL AIRFOIL WITH ACTUATOR SATURATION

Boris Micheli[1]

[1]DLR - German Aerospace Center
Institute of Aeroelasticity, Bunsenstraße 10, 37073 Göttingen (DE)
boris.micheli@dlr.de

Keywords: Aeroservoelasticity, active flutter suppression, actuator saturation, robust control.

Abstract: This paper presents a systematic methodology to evaluate the feasibility of suppressing airplane flutter instabilities through the actively controlled closed-loop actuation of control surfaces in presence of actuator deflection constraints. When active flutter suppression proves to be feasible, the methodology synthesizes a preliminary feedback law able to augment flutter stability of the aeroelastic model under investigation. If active flutter suppression proves to be not viable due to the physical limitations imposed by actuator deflection saturation, the methodology can be employed in a parametric manner to define the actuator performance requirements that would take to implement active flutter suppression. The theoretical background of the methodology is presented and its implementation is validated employing the generic two-dimensional wing section of Theodorsen.

1 INTRODUCTION

The future generation of high-aspect-ratio wings will provide aerodynamic benefits and consequent fuel consumption reduction. However, the increase of the slenderness of the wing will lead to an aircraft configuration more prone to encounter self-excited aeroelastic instabilities, such as flutter [1]. A powerful and effective solution to counteract such aeroelastic instabilities without compromising the structural weight is represented by active flutter suppression (AFS) technologies [2]. AFS technologies could be employed both at the outset of the aircraft design process with the aim of reducing the structural weight of the aircraft [3] and late in the airplane development or service life to counteract flutter problems discovered in these stages which might be impractical or too costly with conventional passive design modifications.

Regardless of the developing stage of an AFS control system and given the safety implication of its potential failure, this technology must be thoroughly understood in all its aspects to allow the careful considerations necessary for its acceptance and verification. To that aim, it is of fundamental relevance to account for control system capability limitations during the design and development phase of the AFS control algorithm. Because of the multidisciplinary nature of an AFS, its capability limitations arise due to the physical nonlinearities of the aeroelastic system (e.g. freeplay control surface nonlinearities, structural damping nonlinearities, aerodynamic nonlinearities involving shock-wave motion and flow separation, etc.) as well as due to the performance limitations and nonlinearities which always characterize actuators and sensors. Among these capability limitations, those caused by actuator saturation nonlinearities deserve a special consideration as they are ubiquitous in aeroservoelasticity. In the specific case of AFS, despite the appearance of high-bandwidth actuators, actuator saturation may arise attempting to deflect the control surfaces at flutter typical frequencies.

The analysis and design of an unstable system that contains saturation nonlinearities is theoretically challenging as well as practically imperative. There are two main strategies to deal with actuator saturation.
The first strategy, which is state of-the-art in industrial applications, is to neglect the saturation nonlinearities in the very first stage of the control design process, and then to add some problem-specific schemes to deal with the adverse effects caused by saturation (e.g. bounded control signals). These schemes, known as anti-windup schemes, present some limitations. Firstly, their synthesis requires *ad hoc* modifications and extensive simulations which generally lead to improved performance but poorly understood stability properties. Secondly, it is not known *a priori* whether the design of a stabilizing feedback law is attainable. In this regard, recent literature [4] has shown that a linear system having poles in the open right-half plane is not globally asymptotically null controllable with bounded control (ANCBC), i.e. for a given bound on the controls, not every state in its state-space can be driven to the origin either in a finite time or asymptotically by a bounded control. Any feedback law designed for such a system would not work globally, but would drive to the origin only a limited set of states, namely the stability would be of a semi-global kind [5].
The second strategy takes into account the saturation nonlinearities at the outset of the control design, thus providing a more systematic approach. This approach entails the characterization of the null controllable region, namely the set of all the states that can be driven to the origin when the input of the system is physically constrained and the design of feedback laws that are valid on the entire region or a large portion of it.

An aircraft flying above the open-loop (OL) flutter speed presents at least a pair of complex conjugated poles in the open right-half plane [2], hence it is not globally ANCBC. With the aim of stabilizing such unstable aeroelastic systems, an approach of the second kind would be advantageous. While the first strategy has been successfully employed in the past to actively suppress flutter in a late stage of the design process [6], to the knowledge of the author, an approach of the second kind has never been attempted and a systematic methodology to assess AFS feasibility from the inception of the aircraft design process has not been presented yet. This is the approach taken in this paper which is based on the recent publications of Hu et al. [7, 8]. In this work, AFS feasibility is intended as the viability to design a control law which is able to achieve semi-global practical stabilization on the null controllable region, where "practical" denotes the ability of the closed-loop (CL) system to reject external disturbances, e.g. atmospheric perturbations. Namely, a minimum disturbance rejection ability is here identified as the crucial factor that discriminates AFS attainability. In order to fulfill this onerous task, the problem of designing an AFS control law considering actuator saturation has been partitioned into three subproblems:

- Design driven by deflection saturation and assessment of rate limit fulfillment in a second step;
- Design driven by rate saturation and assessment of deflection limit fulfillment in a second step;
- Design carried out considering both rate and deflection limits.

The condition listed in the first bullet point forms the frame of this work. The results achieved in this framework and here presented pave the way towards the last two problems, which are subject of current investigations and will be presented in the near future.

The main objective of this paper is to provide a systematic methodology which can be employed to accomplish the tasks enclosed by the dotted line in Fig. 1 and 2 for a generic linear time invariant (LTI) multi-input multi-output (MIMO) aeroelastic plant subjected to actuator

deflection and rate saturation. In particular, the methodology here presented lays the basis for

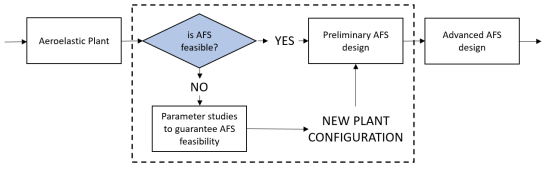

Figure 1: Flowchart of AFS design phase with aircraft design problem formulated in a parametric manner.

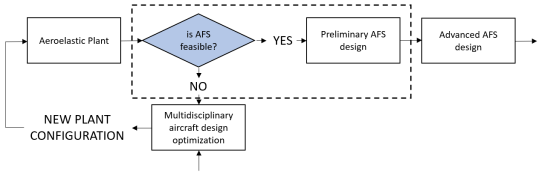

Figure 2: Flowchart of AFS design phase coupled with a multidisciplinary aircraft design optimization environment.

the evaluation of AFS control design feasibility for a generic aeroelastic plant at the outset of the aircraft design.
When AFS proves to be attainable, semi-global practical stabilization of the system is established through a saturated linear state feedback law that meets basic performance and stability requirements and can be used as a starting point for advanced control law design.
Contrarily, parameter studies are carried out to produce a configuration with guaranteed AFS design feasibility [1], as displayed in Fig. 1. The method can also be harnessed and included in a generic multidisciplinary aircraft design optimization environment which provides the new configuration to be analyzed as shown in the flowchart of Fig. 2 (e.g. the DLR parameterized process cpacs-MONA for structural and aeroelastic design [9]).

The paper is organized as follows: In Section 2 the modeling assumptions that lead to the basic LTI MIMO aeroelastic plant to be controlled are discussed. Section 3 introduces the AFS control problem in presence of actuator deflection limits. In particular, Subsection 3.1 introduces the concept of null controllable region, provides its formal definition, and summarizes the main results from the literature which are necessary for its explicit characterization when a generic multiple-input aeroelastic plant experiencing flutter instabilities is under analysis. The control approach employed in this paper is presented in Subsection 3.2 while the theoretical background necessary to evaluate the ability of the feedback law to reject disturbances is introduced in Subsection 3.3. The implemented methodology is successfully applied to a generic two-dimensional wing section and the numerical results are shown and discussed in Section 4. Finally, conclusions and future work are pointed out in Section 5.

2 EQUATIONS OF MOTION OF A GENERIC FLEXIBLE AIRCRAFT MODEL

The primary requirement in aeroservoelasticity is an accurate model suited for the design of advanced control laws. Classic control analyses, design and simulations require the equations of motion (EOM) to be cast in a LTI state-space form. The major technical issue involved in forming the state-space EOM of the aeroservoelastic system is that the generalized aerodynamic forces (GAF) describing the flow over the aircraft are provided within the frequency domain in a tabular form. Therefore, it becomes necessary to convert the frequency-domain description of the GAF in time domain models. This activity is traditionally carried out through rational function approximation (RFA) [10, 11] and, more recently, new possibilities have been opened by the application of tangential interpolation to GAF matrices computed at a prespecified set of reduced frequencies [12, 13]. Regardless of the methodology employed to convert the GAF, the

[1] This is possible only when the design problem is formulated in a parametric manner.

final set of ordinary differential equations (ODE) which define the EOM of a general multiple-input LTI aeroelastic system not subjected to atmospheric disturbances is written as

$$\begin{cases} \dot{\boldsymbol{x}}_{\boldsymbol{pl}}(t) = \mathbf{A}_{\boldsymbol{pl}}\boldsymbol{x}_{\boldsymbol{pl}}(t) + \mathbf{B}_{\boldsymbol{pl}}\boldsymbol{u}_{\boldsymbol{pl}}(t) \\ \boldsymbol{y}_{\boldsymbol{pl}}(t) = \mathbf{C}_{\boldsymbol{pl}}\boldsymbol{x}_{\boldsymbol{pl}}(t) + \mathbf{D}_{\boldsymbol{pl}}\boldsymbol{u}_{\boldsymbol{pl}}(t) \end{cases} \tag{1}$$

where $\boldsymbol{x}_{\boldsymbol{ae}}(t) = \left\{\boldsymbol{u}_{\boldsymbol{h}}(t), \dot{\boldsymbol{u}}_{\boldsymbol{h}}(t), \boldsymbol{x}_{\boldsymbol{a}}(t)\right\} \in \mathbb{R}^n$ is the state vector of the aeroelastic system which comprises the rigid-body states and aircraft structural modes $\boldsymbol{u}_{\boldsymbol{h}}(t)$, their derivatives $\dot{\boldsymbol{u}}_{\boldsymbol{h}}(t)$ as well as the augmented aerodynamic states $\boldsymbol{x}_{\boldsymbol{a}}(t)$ resulting from the conversion, while $\boldsymbol{u}_{\boldsymbol{ae}}(t) = \left\{\boldsymbol{\delta}(t) \quad \dot{\boldsymbol{\delta}}(t) \quad \ddot{\boldsymbol{\delta}}(t)\right\} \in \mathbb{R}^{3\cdot m}$ is the $\boldsymbol{y}_{\boldsymbol{ae}}(t) = \boldsymbol{x}_{\boldsymbol{ae}}(t)$ vector of control surface deflections and related derivatives [2][3].The actuator dynamics of the i^{th} control surface is assumed to be described by a 2^{nd} order LTI system of the form

$$\ddot{\delta}_i(t) + a_{1_i}\dot{\delta}_i(t) + a_{0_i}\delta_i(t) = b_{0_i}\delta_{c_i}(t) \tag{2}$$

where δ_{c_i} is the commanded (input) control surface deflection. Given a generic aircraft provided with m control surfaces, a state-space realization of the m transfer functions (2) leads to the actuator state-space system

$$\begin{cases} \dot{\boldsymbol{x}}_{\boldsymbol{act}}(t) = \mathbf{A}_{\boldsymbol{act}}\boldsymbol{x}_{\boldsymbol{act}}(t) + \mathbf{B}_{\boldsymbol{act}}\boldsymbol{\delta}_{\boldsymbol{c}}(t) \\ \boldsymbol{y}_{\boldsymbol{act}}(t) = \mathbf{C}_{\boldsymbol{act}}\boldsymbol{x}_{\boldsymbol{act}}(t) + \mathbf{D}_{\boldsymbol{act}}\boldsymbol{\delta}_{\boldsymbol{c}}(t) \end{cases} \tag{3}$$

where $\boldsymbol{y}_{\boldsymbol{act}}(t) = \left\{\boldsymbol{\delta}(t) \quad \dot{\boldsymbol{\delta}}(t) \quad \ddot{\boldsymbol{\delta}}(t)\right\}$ is the output vector of the actuator system, and $\boldsymbol{\delta}_c(t) \in \mathbb{R}^m$ is the vector of the commanded control surface deflection. Since systems (1) and (3) are concatenated in a series, i.e. $\boldsymbol{u}_{\boldsymbol{ae}}(t) = \boldsymbol{y}_{\boldsymbol{act}}(t)$, the plant state equation can be written as

$$\underbrace{\begin{Bmatrix} \dot{\boldsymbol{x}}_{\boldsymbol{act}}(t) \\ \dot{\boldsymbol{x}}_{\boldsymbol{ae}}(t) \end{Bmatrix}}_{\dot{\boldsymbol{x}}_{\boldsymbol{pl}}(t)} = \underbrace{\begin{bmatrix} \mathbf{A}_{\boldsymbol{act}} & \mathbf{0} \\ \mathbf{B}_{\boldsymbol{ae}}\mathbf{C}_{\boldsymbol{act}} & \mathbf{A}_{\boldsymbol{ae}} \end{bmatrix}}_{\mathbf{A}_{\boldsymbol{pl}}} \underbrace{\begin{Bmatrix} \boldsymbol{x}_{\boldsymbol{act}}(t) \\ \boldsymbol{x}_{\boldsymbol{ae}}(t) \end{Bmatrix}}_{\boldsymbol{x}_{\boldsymbol{pl}}(t)} + \underbrace{\begin{bmatrix} \mathbf{B}_{\boldsymbol{act}} \\ \mathbf{B}_{\boldsymbol{ae}}\mathbf{D}_{\boldsymbol{act}} \end{bmatrix}}_{\mathbf{B}_{\boldsymbol{pl}}} \boldsymbol{\delta}_{\boldsymbol{c}}(t) \tag{4}$$

where $\boldsymbol{x}_{\boldsymbol{pl}}(t) \in \mathbb{R}^n$ is the state vector of the generic multiple-input plant system to be analyzed and controlled. The polytopic method by Hu and Lin [8] is adopted to represent the actuator saturation nonlinearity and to employ the control methodology proposed in [7] which is reviewed in Section 3. The methodology presents a controller design routine which encounters saturation effects *a priori* assuming δ_{c_i} to be a standard saturation function symmetric with respect to the origin with unitary saturation level. The notation sat is employed to denote this function, i.e.,

$$\mathrm{sat}(s) = \mathrm{sign}(s) \cdot \min\left\{1, |s|\right\}. \tag{5}$$

In order to meet the assumption of unitary saturation level, a normalization of the input signal $\boldsymbol{\delta}_{\boldsymbol{c}}(t)$ is carried out based on an appropriate choice of control surfaces' position limits $\boldsymbol{\delta}_{\boldsymbol{max}}$ to prevent actuator saturation (see Fig. 3). This is the modelling assumption that will lead us to the synthesis of a stabilizing saturated linear state feedback law fulfilling the constraint of deflection limit when AFS proves attainable. Afterwards, a realistic nonlinear actuator model subject to (s.t.) both limitations in deflection and rate is implemented in Simulink (see Fig. 4) as presented by Tang et al [14]. This numerical model will be employed after the design of the AFS feedback law in order to verify the fulfillment of rate limit constraint (RHS decision block of Fig. 5).

[2]In this paper, curly brackets $\left\{\cdot\right\}$ denote column vectors while square brackets $\left[\cdot\right]$ denote matrices and concatenation.

[3]The terms $\boldsymbol{x}_{\boldsymbol{ae}}(t)$, $\boldsymbol{y}_{\boldsymbol{ae}}(t) = \boldsymbol{x}_{\boldsymbol{ae}}(t)$, $\boldsymbol{u}_{\boldsymbol{ae}}(t)$, as well as their components have to be considered as a deviation of the states and the control input from their trimmed conditions.

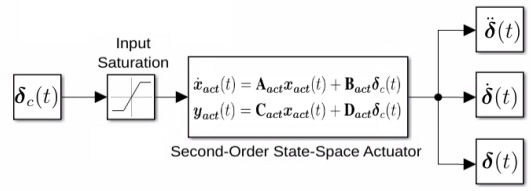

Figure 3: Structure of deflection limit modeling assumptions.

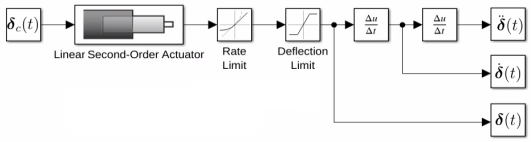

Figure 4: Structure of the realistic nonlinear actuator model.

3 AFS WITH ACTUATOR DEFLECTION LIMITS - PROBLEM FORMULATION

As discussed in Section 2,the LTI multiple-input aeroelastic plant of a generic flexible aircraft model can be written as

$$\dot{\boldsymbol{x}}_{\boldsymbol{pl}}(t) = \mathbf{A}_{\boldsymbol{pl}}\boldsymbol{x}_{\boldsymbol{pl}}(t) + \mathbf{B}_{\boldsymbol{pl}}\,\mathrm{sat}\left(\boldsymbol{\delta}_c(t)\right). \tag{6}$$

Since the magnitude of control surfaces' deflection is physically constrained, certain states cannot be driven to the origin of the phase plane as the required control input might have to be larger than the maximum deliverable deflection $\boldsymbol{\delta_{max}}$. This implies that, despite controllable, the LTI system (6) is not globally null controllable, i.e. it is not possible to steer any of its states to the origin in a finite time by an appropriate choice of the admissible control input. In this situation it is important to identify the set of all the states that can be steered to the origin with the bounded controls delivered by the actuators, i.e. the so-called null controllable region $\mathcal{C}$, and to design a feedback law that works on a large portion of it to address semi-global stabilization on $\mathcal{C}$, while meeting possible design specification on the size of the region of attraction (ROA) $\mathcal{S}^{des}$. Afterwards, it is verified the capability of the CL system to reject external disturbances, namely it is assessed that the synthesized AFS feedback law ensures semi-global practical stabilization on a portion of $\mathcal{C}$. This assessment is carried out formulating the problem in a language of set invariance as described in Subsection 3.3. Finally, to evaluate disturbance rejection capabilities when actuators are also s.t. rate limits, the real actuator model of Fig. 4 is employed. The workflow assumed in this study is depicted by the flowchart of Fig. 5 that describes the internal structure of the dotted line of Fig. 1 and 2. The theoretical background to deal with the processes displayed in Fig. 5 is summarized in the following subsections.

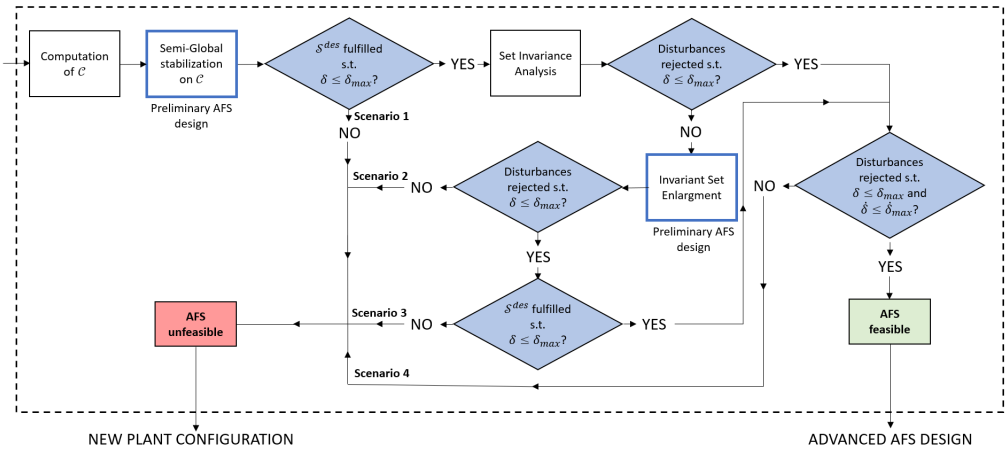

Figure 5: Workflow to discriminate AFS feasibility.

3.1 Computation of null controllable region for a generic LTI multiple-input aeroelastic plant

Given the fundamental role that the null controllable region $\mathcal{C}$ plays in control theory, its characterization is of paramount importance. Considering a linear system of the form of (4), the set of admissible input $\mathcal{U}_a$, also called admissible control, is defined as

$$\mathcal{U}_a = \left\{ \boldsymbol{u} : \boldsymbol{u} \text{ is measurable and } |\boldsymbol{u}(t)|_\infty \leq 1, \forall t \in \mathbb{R} \right\} \tag{7}$$

where $|\boldsymbol{u}(t)|_\infty = \max_i |\boldsymbol{u}_i(t)|$. The objective of defining the set of states that can be steered to the origin by admissible controls leads us to the following

Definition 3.1 (Null Controllable Region)

a) A state $\boldsymbol{x}_0$ is said to be null controllable in time $T > 0$ if there exists an admissible control $\boldsymbol{u}(t)$ such that the state trajectory $\boldsymbol{x}(t)$ of the system satisfies $\boldsymbol{x}(0) = \boldsymbol{x_0}$ and $\boldsymbol{x}(T) = 0$. The set of all states that are null controllable in time T, denoted by $\mathcal{C}(T)$, is called the null controllable region at time T.

b) A state $\boldsymbol{x}_0$ is said to be null controllable if $\boldsymbol{x_0} \in \mathcal{C}(T)$ for some $T \in [0, \infty)$. The set of all null controllable states, denoted by $\mathcal{C}$, is called the null controllable region of the system.

With the above Definition 3.1, the fundamental results on the characterization of the null controllable region are summarized from the literature [15, 16] .

Proposition 3.1 *Assume that $(\boldsymbol{A}, \boldsymbol{B})$ is controllable.*

a) If A is semi-stable, then $\mathcal{C} = \mathbb{R}$;

b) If A is anti-stable, then $\mathcal{C}$ is a bounded convex open set containing the origin;

c) If

$$\boldsymbol{A} = \begin{bmatrix} \boldsymbol{A_{as}} & \boldsymbol{0} \\ \boldsymbol{0} & \boldsymbol{A_{ss}} \end{bmatrix} \tag{8}$$

with $\boldsymbol{A_{as}} \in \mathbb{R}^{n_{as} \times n_{as}}$ anti-stable and $\boldsymbol{A_{ss}} \in \mathbb{R}^{n_{ss} \times n_{ss}}$ semi-stable, and $\boldsymbol{B}$ is partitioned accordingly as

$$\boldsymbol{B} = \begin{bmatrix} \boldsymbol{B_{as}} \\ \boldsymbol{B_{ss}} \end{bmatrix} \tag{9}$$

then,

$$\mathcal{C} = \mathcal{C}_{as} \times \mathbb{R}^{n_{ss}} \tag{10}$$

where $\mathcal{C}_{as}$ is the null controllable region of the anti-stable system

$$\dot{\boldsymbol{x}}_{\boldsymbol{as}}(t) = \boldsymbol{A_{as}} \boldsymbol{x_{as}}(t) + \boldsymbol{B_{as}} \boldsymbol{u}(t) \tag{11}$$

Because of Proposition 3.1, we can concentrate on the study of null controllable regions of anti-stable systems $\mathcal{C}_{as}$, for which, given statement b), the characterization of the boundary $\partial \mathcal{C}_{as}$ is sufficient to describe the set $\mathcal{C}_{as}$ itself. Furthermore, in case of a multiple-input system with m input, let

$$\mathbf{B}(t) = \begin{bmatrix} \mathbf{b_1}(t) & \mathbf{b_2}(t) & \dots & \mathbf{b_m}(t) \end{bmatrix}$$

and for each $i = 1$ to m, let the null controllable region of the system

$$\dot{\boldsymbol{x}}(t) = \mathbf{A}\boldsymbol{x}(t) + \mathbf{b_i} \boldsymbol{u_i}(t)$$

be $\mathcal{C}_i$, then

$$\mathcal{C} = \sum_{i=1}^{m} \mathcal{C}_i = \left\{ \boldsymbol{x_1}(t) + \boldsymbol{x_2}(t) + \dots \boldsymbol{x_m}(t) : \boldsymbol{x_i}(t) \in \mathcal{C}_i, i = 1, 2, \dots, m \right\}. \tag{12}$$

Eq. (12) establishes that null controllable region of a generic multi-input system can be constructed starting from the region $\mathcal{C}_i$ computed considering the system as it was single-input. In view of the above-mentioned considerations, we can restrict, without loss of generality, the study of null controllable regions to single-input anti-stable systems. Focusing on aeroelastic systems, any multiple-input aeroelastic plant described in the form of Eq. (3) can be recasted in form of Eq. (8) (9) through an appropriate state transformation $\boldsymbol{x} = \mathbf{T} \begin{bmatrix} \boldsymbol{x_{as}}(t) & \boldsymbol{x_{ss}}(t) \end{bmatrix}^T$, namely can be partitioned into its anti-stable and semi-stable part. The state-transformation matrix $\mathbf{T}$ can be computed employing the stable algorithm based on Real Schur Decomposition Technique developed by Singh and Nagar [17]. Application of Eq. (12) is afterwards straightforward. Finally, an aeroelastic plant operating above the OL flutter speed V_{fl}^{OL} presents, at least, a pair of complex conjugated poles with positive real part. For the particular case of single-input anti-stable systems with complex conjugated eigenvalues, an explicit description of $\partial\mathcal{C}_{as}$ has been derived in [8]:

$$\partial\mathcal{C}_{as} = \pm e^{-\mathbf{A_{as}}t} \boldsymbol{z_s^-} - \int_0^t e^{-\mathbf{A_{as}}(t-\tau)} \mathbf{b_{as}} d\tau \ : \ t \in [0, T_p) \tag{13}$$

where the terms $\boldsymbol{z_s^-}$ and T_p are functions of $\mathbf{A_{as}}$ and $\mathbf{b_{as}}$ and their calculations can be found in the reference. It is worthy to remark that $\partial\mathcal{C}_{as}$ is not affected by the applied control law, but only depends on the dynamics of the unstable states which is governed by the pair ($\mathbf{A_{as}}$, $\mathbf{b_{as}}$). Based on Proposition 3.1 and Eq. (12) (13)) it is possible to establish an explicit description of $\mathcal{C}$ for a generic multiple-input aeroelastic plant.

3.2 Semi-global stabilization on null controllable region

In planning the safe operation of a nonlinear system an estimation of the ROA $\mathcal{S}$ of an equilibrium point is required. This is of practical importance, since controllers for safety-critical systems are required to guarantee safety over a certain domain of operation, before they can be implemented on the real system. It is obvious from Subsection 3.1 that $\mathcal{C}$ delineates the upper boundary of the ROA $\mathcal{S}$ of the origin of the phase plane. Consequently, when the size of the ROA is a design specification, it is possible to fulfill the requirements only when $\mathcal{S}^{des} \subset \mathcal{C}$. Given an unperturbed aeroelastic plant of generic order flying above the OL flutter speed V_{fl}^{OL}, it is possible to construct a feedback law that leads to a ROA that contains any a priori given bounded subset of the null controllable region in its interior based on the semiglobal stabilization strategy for exponentially unstable linear systems with saturating actuators, as presented by Hu et al. [7].
The key feature of this strategy is to define the set $\Omega = \Omega_{as}(\gamma_{as}) \times \Omega_{ss}(\gamma_{ss})$, with $\Omega_{as}(\gamma_{as}) \in \mathbb{R}^{n_{as}}$ and $\Omega_{ss}(\gamma_{ss}) \in \mathbb{R}^{n_{ss}}$, and to build a saturated linear state feedback law that guarantees Ω to be contained in the ROA of the CL system. The size of Ω depends on the parameters γ_{as} and γ_{ss} that are selected to meet the design specification. The EOM of the CL system read

$$\dot{\boldsymbol{x}}_{\boldsymbol{pl}}(t) = \mathbf{A_{pl}} \boldsymbol{x_{pl}}(t) + \mathbf{B_{pl}} \boldsymbol{\delta_c}(t), \quad \boldsymbol{\delta}_c(t) = \begin{cases} \mathrm{sat}(k \boldsymbol{f_0} \boldsymbol{x_{as}}(t)), & \boldsymbol{x_{pl}}(t) \notin \mathcal{D}(\varepsilon) \\ \mathrm{sat}(\boldsymbol{f}(\varepsilon) \mathbf{T} \boldsymbol{x_{pl}}(t)), & \boldsymbol{x_{pl}}(t) \in \mathcal{D}(\varepsilon) \end{cases} \tag{14}$$

where k, $\boldsymbol{f}$, $\boldsymbol{f_0}$, ε are defined in [7], $\mathcal{D}(\varepsilon)$ is the larger invariant set where the control $\boldsymbol{\delta_c}(t)$ works in the linear region and, for the sake of simplicity, all the states are assumed to be available for

feedback design. It has to be highlighted that the here-employed stabilization strategy solves an algebraic Riccati equation which is nearing associated with the minimum energy regulation problem, as the selected state weighting matrix $\boldsymbol{Q}$ is assumed equal to $\varepsilon \boldsymbol{I}$, with ε of the order of 10^{-6}. Regulator design with zero-state weighting leaves the stable poles unchanged and reflects unstable poles about the imaginary axes. This approach may be of concern in the design of flutter suppression systems for aeroelastic plants in which there may be marginally unstable modes, i.e. modes having low damping ratio. This is often the scenario at flying speed near V_{fl}^{OL}. Moreover, the method cannot be used to improve damping of subcritical flutter modes, namely marginally stable poles. In these cases the stabilization strategy can be employed in conjunction with a methodology described by Anderson and Moore [16] to solve the regulator problem with a prescribed degree of stability. The next question is how to assess disturbance rejection capabilities with saturation nonlinearities present.

3.3 Set-invariance analysis and invariant set enlargement

The well-known fact that the ROA of an equilibrium point is an invariant set [18] guarantees for the nominal system defined by Eq. (14) that any trajectory starting in $\Omega \subset \mathcal{S}$ will go to the origin under the saturated linear state feedback law. However, the stabilizing control law was designed without accounting the disturbances that unavoidably enter in the control loop. The primary concern of this section is the boundedness of the states trajectories of system (14) in presence of non-input additive disturbances of the form

$$\dot{\boldsymbol{x}}_{\boldsymbol{pl}}(t) = \mathbf{A}_{\boldsymbol{pl}}\boldsymbol{x}_{\boldsymbol{pl}}(t) + \mathbf{B}_{\boldsymbol{pl}}\,\mathrm{sat}(\mathbf{F}\boldsymbol{x}_{\boldsymbol{pl}}(t)) + \mathbf{B}_{\boldsymbol{d}}\boldsymbol{w}(t) \tag{15}$$

where $\mathrm{sat}(\mathbf{F}\boldsymbol{x}_{\boldsymbol{pl}}(t))$ represents the saturated feedback law described in Eq. (14) and $\boldsymbol{w}(t) \in \mathbb{R}^q$ is the disturbance. For simplicity and without loss of generality we assume that the bounded disturbance $\boldsymbol{w}(t)$ belongs to the set

$$\mathcal{W} = \left\{\boldsymbol{w} : \boldsymbol{w}(t)^T\boldsymbol{w}(t) \leq 1, \forall t \geq 0\right\}. \tag{16}$$

Since the term $\mathbf{B}_{\boldsymbol{d}}\boldsymbol{w}(t)$ in Eq. (15) is outside of the saturation function, if $\mathbf{B}_{\boldsymbol{d}}$ is sufficiently large, it may be impossible to keep the trajectory of the states bounded, no matter where it starts and whatever control is applied. Hence, it is required to the CL system to have an invariant set $\mathcal{E}(\mathbf{P}_{\mathbf{1}}, \rho)$ (i.e. all the trajectories starting from $\mathcal{E}(\mathbf{P}_{\mathbf{1}}, \rho)$ will remain inside it regardless of $\boldsymbol{w}(t) \in \mathcal{W}$), where $\mathbf{P}_{\mathbf{1}} \in \mathbb{R}^{n\times n}$ is a positive definite matrix and $\mathcal{E}(\mathbf{P}_{\mathbf{1}}, \rho)$ is an ellipsoid set defined by

$$\mathcal{E}(\mathbf{P}_{\mathbf{1}}, \rho) := \left\{\boldsymbol{x} \in \mathbb{R}^2 : \boldsymbol{x}^T\mathbf{P}_{\mathbf{1}}\boldsymbol{x} \leq \rho\right\}. \tag{17}$$

The invariant ellipsoid $\mathcal{E}(\mathbf{P}_{\mathbf{1}}, \rho)$ provides an estimation of the ROA of system (15), i.e. an estimation of the ROA when disturbances are accounted. The problem becomes how to identify the largest invariant ellipsoid $\mathcal{E}(\mathbf{P}_{\mathbf{1}}, \rho)$ to achieve the least conservative estimate. The set invariant conditions for system (15) are given by the following theorem:

Theorem 3.1 *For a given ellipsoid $\mathcal{E}(\boldsymbol{P}, \rho)$, if there exist an $\boldsymbol{H} \in \mathbb{R}^{m\times n}$ and a positive number η such that $\forall i \in [1, 2^m]$*

$$\big(\boldsymbol{A} + \boldsymbol{B}(\boldsymbol{D_i}\boldsymbol{F} + \boldsymbol{D_i^-}\boldsymbol{H})\big)^T\boldsymbol{P} + \boldsymbol{P}\big(\boldsymbol{A} + \boldsymbol{B}(\boldsymbol{D_i}\boldsymbol{F} + \boldsymbol{D_i^-}\boldsymbol{H})\big) + \frac{1}{\eta}\boldsymbol{P}\boldsymbol{B_d}\boldsymbol{B_d^T}\boldsymbol{P} + \frac{\eta}{\rho}\boldsymbol{P} \leq 0 (< 0) \tag{18}$$

and $\mathcal{E}(\boldsymbol{P},\rho)\subset\mathcal{L}(\boldsymbol{H})$, then $\mathcal{E}(\boldsymbol{P},\rho)$ is a (strictly) invariant set for the system (15) [4].

Based on Theorem 3.1, Hu and Lin [8] propose the following optimization problem to identify the largest invariant ellipsoid $\mathcal{E}(\mathbf{P_1},\rho)$

$$\sup_{\mathbf{P_1}>0,\rho,\eta>0,\boldsymbol{H}} \quad \alpha_1 \tag{19}$$
subject to
a) $\alpha_1\mathcal{X}_0\subset\mathcal{E}(\mathbf{P_1},\rho)$;
b) Inequality (18) holds, $\forall i=1,2,\ldots,n$
c) $|\boldsymbol{h}_i\boldsymbol{x}|\leq 1,\quad \forall\boldsymbol{x}\in\mathcal{E}(\mathbf{P_1},\rho),\quad i\in[1,m]$.
where $\mathcal{X}_0$ is a given reference ellipsoid $\mathcal{E}(\mathbf{R_0},1)$, and constraint c) reshapes the condition $\mathcal{E}(\mathbf{P_1},\rho)\subset\mathcal{L}(\mathbf{H})$ by using the Lagrange multiplier method.

Problem (19) is reformulated in the following convex optimization problem with Linear Matrix Inequalities (LMIs) constraints employing Schur's complement. The exhaustive formulation of the problem is found in [8].

$$\min_{\boldsymbol{Q}>0,\rho,\eta>0,\boldsymbol{Z}} \quad \gamma \tag{20}$$
subject to
a) $\begin{bmatrix}\gamma\mathbf{R} & \mathbf{I}\\ \mathbf{I} & \mathbf{Q}\end{bmatrix}\geq 0$;
b) $\mathbf{Q}\mathbf{A}^T+\mathbf{A}\mathbf{Q}+(\mathbf{D_i}\mathbf{Y}+\mathbf{D_i^-}\mathbf{Z})^T\mathbf{B}^T+\mathbf{B}(\mathbf{D}_i\mathbf{Y}+\mathbf{D_i^-}\mathbf{Z})+\frac{1}{\eta}\mathbf{B_d}\mathbf{B_d}^T\frac{\rho}{\eta}\mathbf{Q}<0,\quad i\in[1,2^m]$
c) $\begin{bmatrix}1 & \mathbf{z_i}\\ \mathbf{z_i}^T & \boldsymbol{Q}\end{bmatrix}\geq 0,\quad i=1,2,\ldots,m$;
where $\gamma=\frac{1}{\alpha_1^2}$, $Q=(\frac{\mathbf{P_1}}{\rho})^{-1}$, $\mathbf{Y}=\mathbf{F}\mathbf{Q}$, and $\mathbf{Z}=\mathbf{H}\mathbf{Q}$.

The set invariance Problem (20) can be readily solved by convex optimization tools. In particular, the global minimum of γ is obtained by running $\frac{\rho}{\eta}$ from 0 to ∞, while ρ is set to $\rho=1$ as it can be absorbed into other parameters. If the optimization Problem (20) is feasible, then the stabilizing control law $\mathrm{sat}(\mathbf{F}\boldsymbol{x_{pl}}(t))$ is able to guarantee semi-global practical stabilization on $\mathcal{E}(\mathbf{P_1},\rho)$ when actuator deflection limits are accounted. On the contrary, disturbance rejection is not guaranteed by the designed feedback law. Under the latter scenario it is necessary to seek for a feedback law $\mathbf{F}$ that maximizes the size of $\mathcal{E}(\mathbf{P_1},\rho)$. Here, this maximization is carried out only on the anti-stable part of the system, i.e. solving Problem (20) with $(\mathbf{A},\mathbf{B},\mathbf{B_d})=(\mathbf{A_{as}},\mathbf{B_{as}},\mathbf{B_{d_{as}}})$ and $\mathbf{F}$ as an additional unknown parameter. When a solution is found, the result will be an optimized feedback law $\boldsymbol{f_{as}^{opt}}\in\mathbb{R}^{n_{as}}$ that will be employed in Eq. (14) to stabilize the anti-stable dynamics of the system, when not, semi-global practical stabilization is proven unfeasible. Finally, in the former case, it is necessary to verify the fulfillment of a possible design specification $\mathcal{S}^{des}$ on the size of the ROA. This last assessment might not be fulfilled, resulting in a AFS unfeasible scenario of the 3^{rd} kind (see Fig. 5).

[4] Denoting $\mathcal{D}$ the set of $n\times n$ diagonal matrices whose diagonal elements are either 1 or 0, there are 2^n elements in $\mathcal{D}$ and each of them is labelled as $\mathbf{D_i}$, $i=1,2,\ldots,n$. $\mathbf{D_i^-}$ indicates the matrix $\mathbf{I}-\mathbf{D_i}$ which is also clearly an element of $\mathcal{D}$.
$\mathcal{L}(\mathbf{H})$ denotes the linear region of the saturation function $\mathrm{sat}(\mathbf{H}\boldsymbol{x_{pl}}(t))$ which is defined as $\mathcal{L}(\mathbf{H}):=\left\{\boldsymbol{x}\in\mathbb{R}^n:|\boldsymbol{h_i}\boldsymbol{x}|\leq 1,i=1,2,\ldots,m\right\}$ with $\boldsymbol{h_i}$ denoting the $i-th$ row of $\mathbf{H}$.

4 NUMERICAL RESULTS

The methodology presented in Section 3 is applied to the generic two-dimensional wing section of Theodorsen [19] in order to demonstrate its viability. The recasting of the EOM in a LTI state-space form is achieved employing the RFA of the generalized Theodorsen function derived by Jones [20]. The resulting state-space equations that describe the dynamics of the wing section around its equilibrium point read

$$\underbrace{\begin{Bmatrix} \dot{\boldsymbol{\xi}}(t) \\ \ddot{\boldsymbol{\xi}}(t) \\ \dot{\boldsymbol{x}}_{\boldsymbol{a}}(t) \end{Bmatrix}}_{\dot{\boldsymbol{x}}_{\boldsymbol{ae}}(t)} = \mathbf{A}_{\boldsymbol{ae}} \underbrace{\begin{Bmatrix} \boldsymbol{\xi}(t) \\ \dot{\boldsymbol{\xi}}(t) \\ \boldsymbol{x}_{\boldsymbol{a}}(t) \end{Bmatrix}}_{\boldsymbol{x}_{\boldsymbol{ae}}(t)} + \mathbf{B}_{\boldsymbol{ae}} \underbrace{\begin{Bmatrix} \beta(t) \\ \dot{\beta}(t) \\ \ddot{\beta}(t) \end{Bmatrix}}_{\boldsymbol{u}_{\boldsymbol{ae}}(t)} + \mathbf{B}_{\boldsymbol{d_{ae}}} \underbrace{\boldsymbol{f}_{\boldsymbol{g}}(t)}_{\boldsymbol{w}_{ae}(t)} \tag{21}$$

where $\boldsymbol{\xi}(t) = \begin{Bmatrix} h(t)/b & \alpha(t) \end{Bmatrix} \in \mathbb{R}^2$, $\boldsymbol{x_a}(t) \in \mathbb{R}^4$ as a result of the employed RFA which is characterized by only two aerodynamic poles. The vector $\boldsymbol{u_{ae}}(t) = \begin{Bmatrix} \beta(t) & \dot{\beta}(t) & \ddot{\beta}(t) \end{Bmatrix}$ represents the aileron deflection and its relative derivatives in agreement with the original Theodorsen's notation, while $\boldsymbol{f_g}(t) = \begin{Bmatrix} L_g(t) & M_g(t) \end{Bmatrix}$ denotes the incremental lift and moment distribution due to atmospheric disturbances. The time evolution of $\boldsymbol{f_g}(t)$ is computed simulating the second order LTI system

$$\begin{cases} \dot{\boldsymbol{x}}_{\boldsymbol{g}}(t) = \mathbf{A}_{\boldsymbol{g}} \boldsymbol{x}_{\boldsymbol{g}}(t) + \mathbf{B}_{\boldsymbol{g}} w_g(t) \\ \boldsymbol{f}_{\boldsymbol{g}}(t) = \mathbf{C}_{\boldsymbol{g}} \boldsymbol{x}_{\boldsymbol{g}}(t) + \mathbf{D}_{\boldsymbol{g}} w_g(t) \end{cases} \tag{22}$$

by means of the LSIM-H algorithm [21]. System 22 is based on the RFA of Küssner's function for incompressible flow developed by von Karman and Sears [22]. The term $w_g(t)$ describes the vertical wind velocity distribution and in in this study is characterized considering two categories of disturbances: $1 - cos$ discrete gusts, representative of finite energy disturbances, and continuous turbulence (CT), that serves as a persistent disturbance. For the former case, the gust profile is taken as established by the EASA Certification Specifications [23] considering eight different gust gradient distances ranging from 9 m to 107 m. For the latter case, the stochastic time evolution of $w_g(t)$ can be determined projecting a normally distributed univariate random variable on the frequency domain through a Fast Fourier Transform (FFT) process, filtering the projected signal by a Von Karman's spectrum [24], and reversing back the filtered signal through Inverse Fast Fourier Transform (IFFT). The discrete gust considered in this study and an example of the so-achieved turbulence signal in time domain of moderate severity (the probability of the turbulence intensity being exceeded is selected as 10^{-3} which results in a turbulence intensity $\sigma_w \approx 10$ ft/s at an altitude of 10000 ft [24]) are displayed in Fig. 6. The explicit description of $\mathbf{A_g}$, $\mathbf{B_g}$, $\mathbf{C_g}$, and $\mathbf{D_g}$ is found in [25]. Matrices $\mathbf{A_{ae}}$, $\mathbf{B_{ae}}$, and $\mathbf{B_{d_{ae}}}$

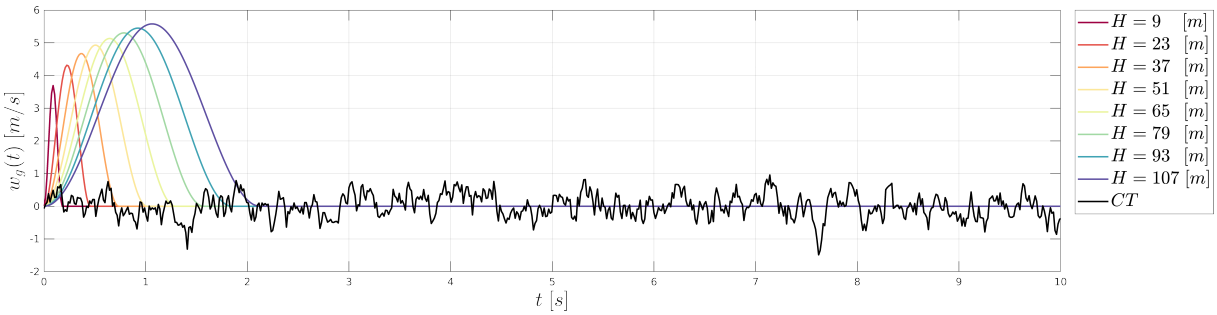

Figure 6: Discrete gust profiles and example of turbulence filtered signal by Karman's spectrum in time domain.

appearing in Eq. (21) are computed recasting the augmented state space model presented in [26]

and the numerical values of the structural and geometrical parameters for their computation is also found in the reference. In particular, the aileron spans 20% of the chord and the bending-torsion frequency ratio ω_h/ω_α, that has a strong influence on the flutter characteristics, is taken as $\omega_h/\omega_\alpha = 0.5$.
The reference actuator model of the trailing edge control surface of the BACT wind tunnel model [27] is employed to characterize Eq. (2). The deflection and rate limits will be imposed in the following subsections. The concatenation of the BACT wing actuator dynamics with Eq. (21) leads to the state-space equations of the aeroelastic plant

$$\dot{\boldsymbol{x}}_{\boldsymbol{pl}}(t) = \boldsymbol{A}_{\boldsymbol{pl}}\boldsymbol{x}_{\boldsymbol{pl}}(t) + \boldsymbol{B}_{\boldsymbol{pl}}\beta_c(t) + \mathbf{B}_{\boldsymbol{d}_{\boldsymbol{pl}}}\boldsymbol{f}(t) \tag{23}$$

where $\boldsymbol{x}_{\boldsymbol{pl}}(t) = \begin{Bmatrix}\beta(t) & \dot{\beta}(t) & \boldsymbol{\xi}(t) & \dot{\boldsymbol{\xi}}(t) & \boldsymbol{x}_{\boldsymbol{a}}(t)\end{Bmatrix} \in \mathbb{R}^{10}$. The eigenvalues of $\boldsymbol{A}_{\boldsymbol{pl}}$ are approximate roots of the aeroelastic plant EOM. Figure 7 compares these eigenvalues to the exact roots of the EOM which are computed by means of a description of the GAF in the full Laplace domain employing the generalized Theodorsen's function as presented by Edwards [26]. Both the exact and approximated solution show that the bending branch goes across the imaginary axes becoming unstable at the true-air-speed $V_{fl}^{OL} = 91.8$ m/s. From the close agreement between the exact and the approximate roots, it is concluded that the here described LTI state-space model is able to capture the dynamics of the system, hence it is suitable for the purpose of control design.

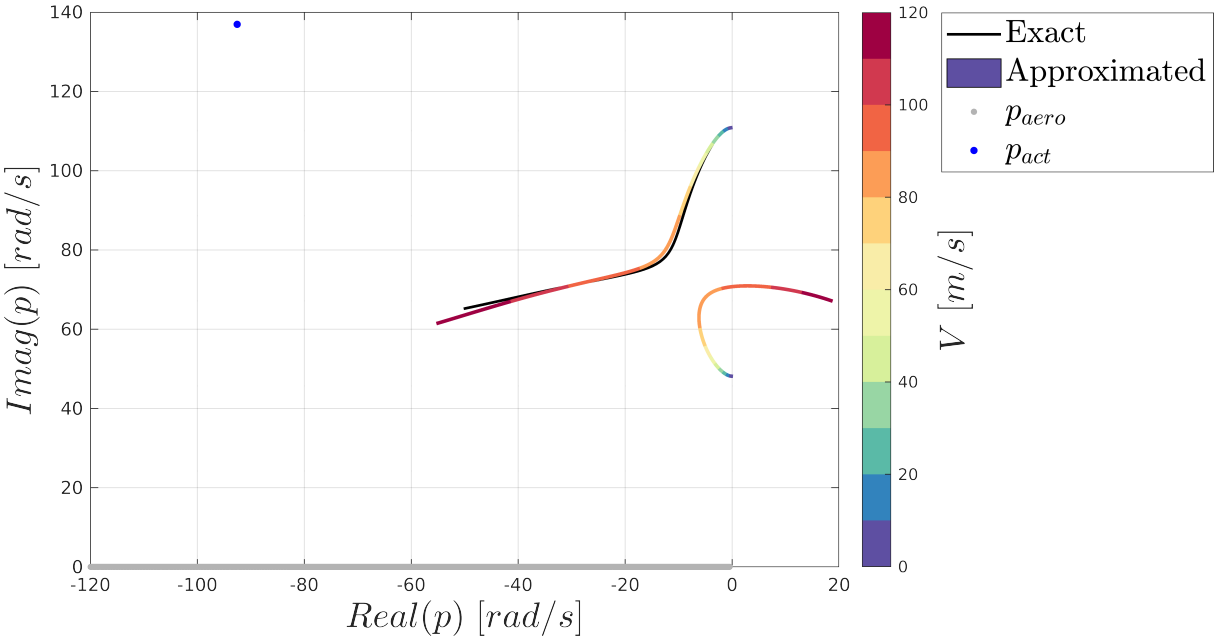

Figure 7: Comparison of poles obtained using the generalized Theodorsen function (exact poles) and Jones' RFA (approximated poles).

4.1 Example of feasible AFS

In this subsection the physical limits of the trailing edge control surface actuator of the BACT wing are employed to investigate the feasibility of AFS and, possibly, to synthesize a preliminary controller to ensure that 1) the states of the system are bounded and asymptotically converge to the origin, 2) the ROA $\mathcal{S}$ of the CL unperturbed system must enclose the ball $\mathcal{X}^{des} = \{\boldsymbol{x} \in \mathbb{R} : |\boldsymbol{x}| \leq 6\}$ (condition on $\mathcal{S}^{des}$), 3) the CL system has an invariant set $\mathcal{E}(\mathbf{P_1}, \rho)$, so that all the states trajectories starting from $\mathcal{E}(\mathbf{P_1}, \rho)$ (in particular, the origin) will remain in it.

The deflection limit is measured to be $\beta_{max} = 12$ deg, while rate limit has not been determined [27], presumably not proving troublesome during the experimental campaign. Therefore, it is reasonable to carry out a control design procedure driven by the deflection limit. In a second stage, a value of $\dot{\beta}_{max} = 50$ deg/s is assumed to assess rate limit fulfillment.
The selected design speed is $V_{des} = \sqrt{1.2} V_{fl}^{OL} \approx 100.5$ m/s, namely 20% higher than the OL flutter dynamic pressure q_{fl}^{OL}. At this flight point the system presents a pair of complex conjugated unstable poles $p = 7.66 + i70.53$ rad/s due to the bending mode instability (see Fig. 7). To suppress flutter, a feedback law is designed according to the synthesis procedure summarized in Subsection 3.2. After having performed an input normalization such that the control is bounded by 1 and having applied the stable-unstable decomposition algorithm [17], it is taken $\gamma_{as} = 0.92$ for the anti-stable subsystem to generate a set $\Omega_{as}(\gamma_{as})$ such that $\mathcal{X}_{as}^{des} \subset \Omega_{as}(\gamma_{as})$ to fulfill design condition 2 (see Fig. 8). With the synthesis technique presented in [8] a feedback $\beta_c(t) = \text{sat}(k\boldsymbol{f_0 x_{as}}(t))$ is obtained such that $\Omega_{as}(\gamma_{as})$ is inside the ROA of the anti-stable subsystem. Despite the steady-stable subsystem being stable, the synthesis procedure computes the full state feedback $\beta_c(t) = \text{sat}(k\boldsymbol{f}(\varepsilon)\mathbf{T}\boldsymbol{x_{pl}}(t))$ to be applied when $\boldsymbol{x_{pl}}(t) \in \mathcal{D}(\varepsilon)$ to guarantee $\Omega_{as}(\gamma_{as}) \times \Omega_{ss}(\gamma_{ss}) \subset \mathcal{S}$. A value of $\gamma_{ss} = 6$ was selected in agreement with design condition 2. In Fig. 8, the relevant sets as well as the ball $\mathcal{X}^{des}$ are projected on the anti-stable phase plane. The outermost closed curve is the boundary of the null controllable region $\mathcal{C}_{as}$, the inner dash-dotted closed curve is $\Omega_{as}(\gamma_{as})$ which clearly encloses the ball $\mathcal{X}^{des}$, and the innermost dotted closed curve is $\mathcal{D}_{as}(\varepsilon)$. The CL unperturbed system is able to drive to the origin any initial state $\boldsymbol{x_{pl_0}} \in \Omega_{as}(\gamma_{as}) \times \Omega_{ss}(\gamma_{ss})$ while fulfilling $|\beta_c| \leq \beta_{max}$. To prove the capability of the controller to stabilize the airfoil pitch and bending motion, a pulse excitation $\beta_c(t) = (t/t_0)^2 e^{2-1/(1-t/t_0)}$ with $t_0 = 0.5$ s resulting in a peak value of $\max(\beta_c(t)) = 3$ deg is applied to trigger oscillations while the activation of the AFS controller is delayed by $\tau = 0.5$ s. The open- and closed-loop responses of the system at V_{des} as well as the projection of the states trajectories on the anti-stable phase plane are given in Fig. 9. As shown, after the activation

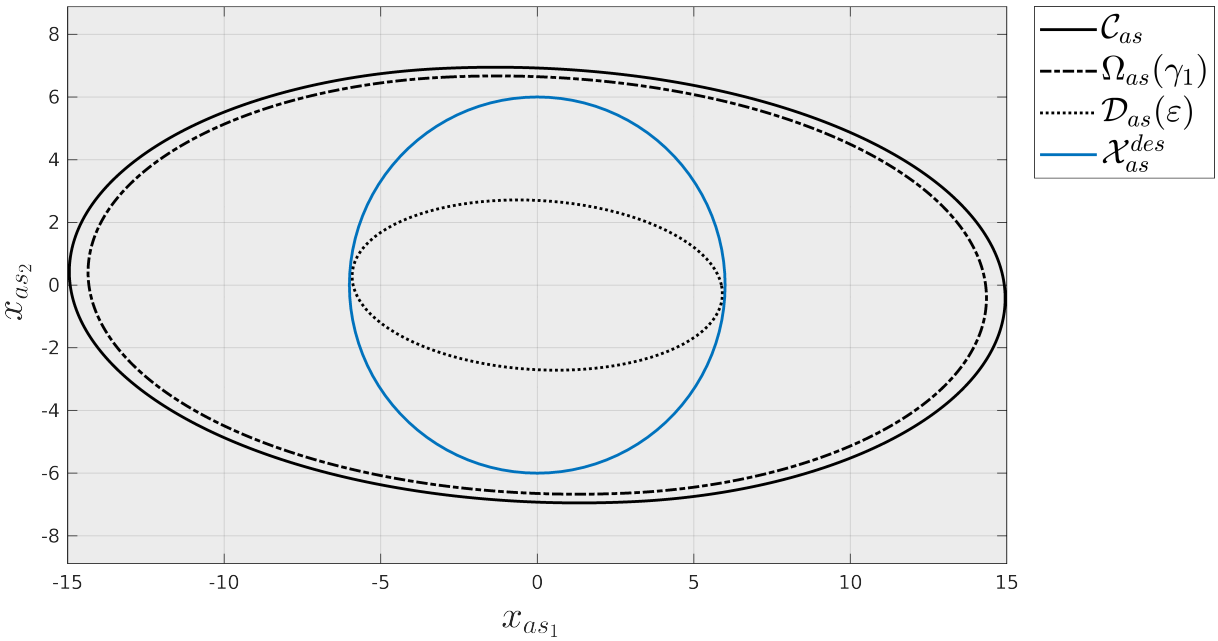

Figure 8: Projection of relevant system sets on anti-stable phase plane.

of the AFS controller, both the bending motion $h(t)/b$ and the pitch angle $\theta(t)$ are settle down smoothly, preventing the divergence of the oscillations that instead occurs for the OL system. The rate saturation encountered when simulating the system with the real actuator model of Fig.

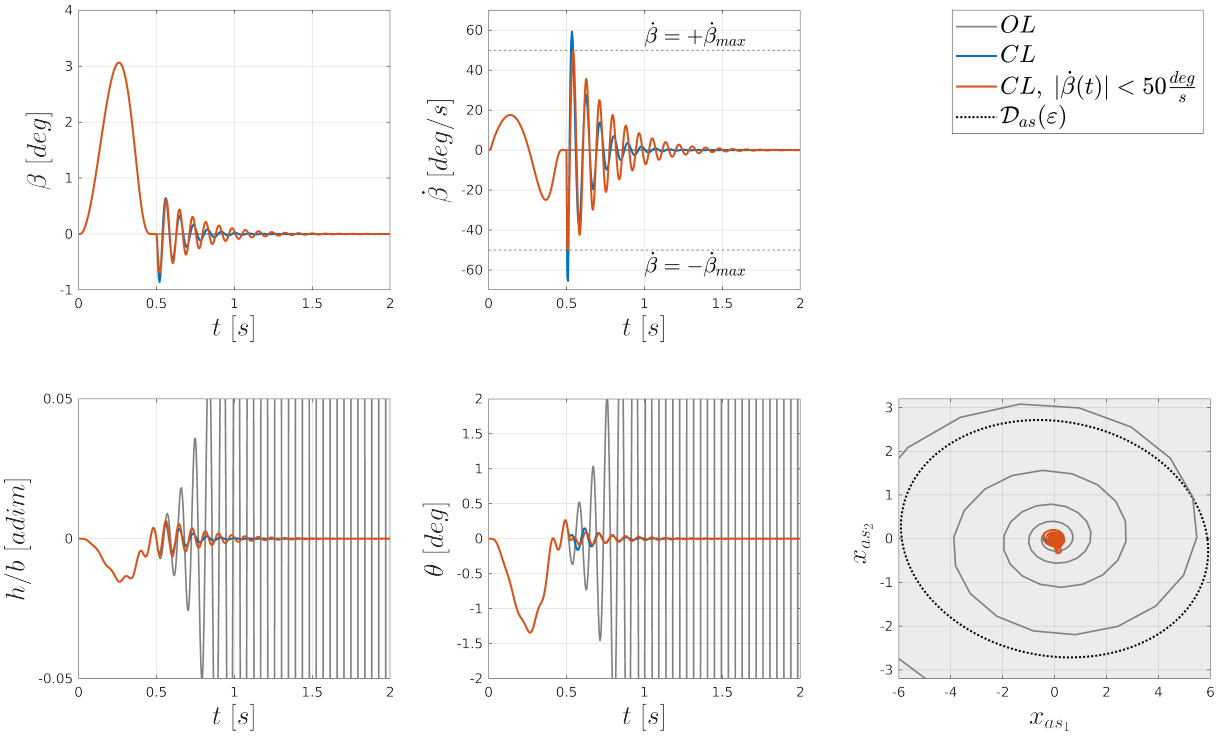

Figure 9: Time evolution of the wing section for a 3 deg deflection pulse of the aileron with AFS control law activation delayed by $\tau = 0.5$ s at V_{des} and projection of state trajectories on anti-stable phase plane.

4 is related to the imposed delay as well as to the abrupt switch on of the AFS controller that are not likely in a real application where AFS is constantly active.

The assessment of disturbance rejection performances of the designed AFS control law involves a normalization of the disturbance $\boldsymbol{f_g}(t)$ to fulfill Eq. (16). In case of a CT encounter the normalization factor of each component is taken as three times their standard deviation, i.e. $\mathbf{K_{norm}} = 3{\cdot}\mathrm{diag}(\sigma(L_g(t)), \sigma(M_g(t)))^{-1} = \mathrm{diag}(117.0\ \mathrm{N/m}, 3.6\ \mathrm{N/m^2})^{-1}$, corresponding to the distributed load values with an exceedance probability of 0.3%. The projection of the resulting ROA on the anti-stable phase plane $\mathcal{E}_{as}(\mathbf{P_1}, 1)$ of the so-perturbed system computed solving the LMI optimization Problem (20), is depicted by the blue dotted line in Fig. 10. The third design objective has been achieved and the boundedness of the states is ensured. However, asymptotic convergence of the states to the origin cannot be achieved in case of CT encounters. All the trajectories starting from $\mathcal{E}_{as}(\mathbf{P_1}, 1)$ will enter $\mathcal{E}_{as}(\mathbf{P_2}, 1)$, displayed with orange dotted line, in finite time, but will never be steered to the origin due to the persistent disturbance. The invariant set $\mathcal{E}_{as}(\mathbf{P_2}, 1)$ is computed solving Problem (19), but seeking for $\inf(\alpha_2)$ and changing constraint a) into $\mathcal{E}_{as}(\mathbf{P_2}, \rho) \subset \alpha_2 \mathcal{X}_\infty$ (compare to the so-called Disturbance Rejection Problem [8]). In particular, $\mathcal{E}_{as}(\mathbf{P_2}, 1) \subset \alpha_2 \mathcal{E}_{as}(\mathbf{I}, 1)$ with $\alpha_2 = 1.03$ which shows that the disturbance cannot be rejected to a very small level. Nevertheless, since Problem (20) has a solution, AFS feasibility is guaranteed and an improvement of disturbance rejection capability can be carried out in a second stage of the control design process if deemed required.

Secondly, the capability of the system to reject discrete gusts is analyzed. The normalization factor is taken as $\mathbf{K_{norm}} = \mathrm{diag}(\max(L_g(t)), \max(M_g(t)))^{-1}$ for all the different values of gust gradient distances considered (see Fig. 6). Results are displayed in Fig. 11. Gusts with high gradient distance appear more critical than CT for the definition of the ROA of the perturbed system (23), which overall is represented by the invariant set $\mathcal{E}_{as}(\mathbf{P_1}, 1)$ associated to a gust with gradient distance of 107 m. However, it is also important to highlight that Problem (20) relies on Theorem 3.1, which is extremely conservative for finite energy perturbations such as discrete

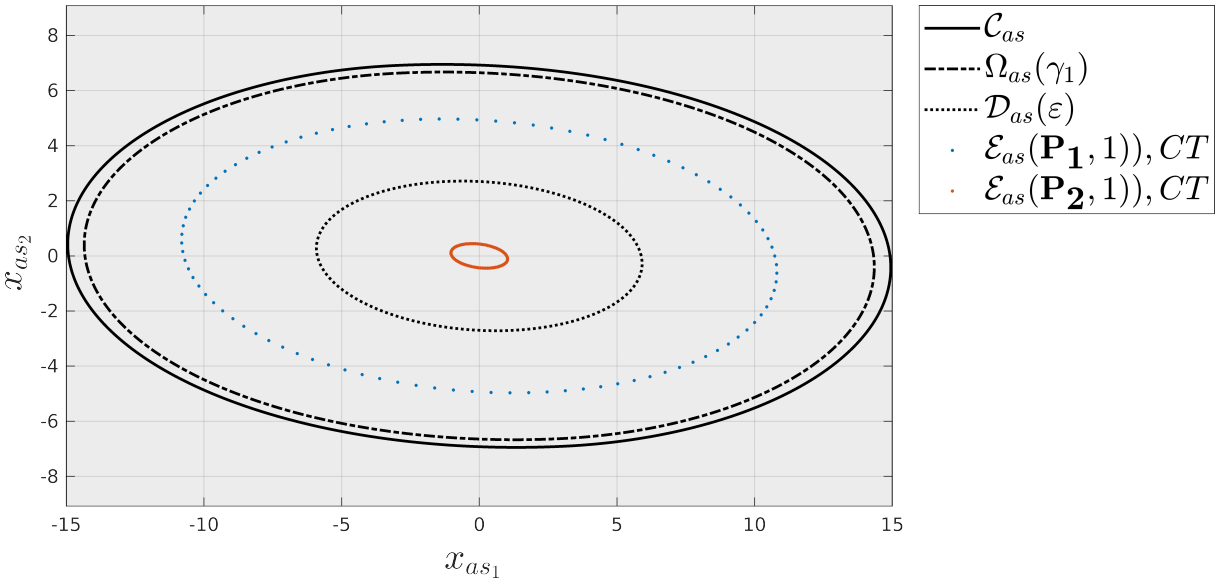

Figure 10: Projection of invariant ellipsoids associated with CT disturbances on the anti-stable phase plane.

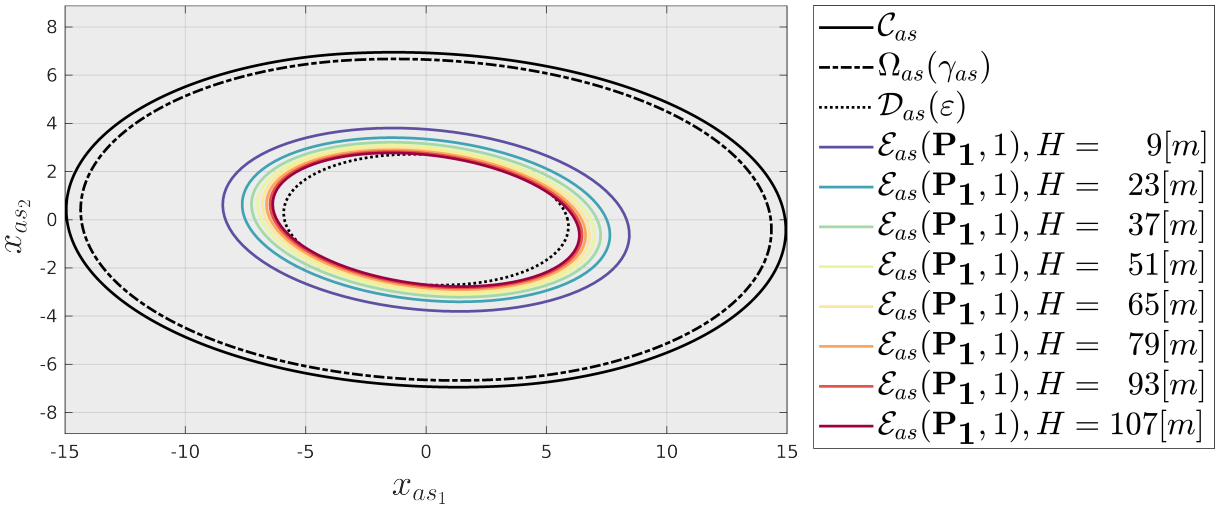

Figure 11: Projection of invariant ellipsoids associated with discrete gust disturbances on the anti-stable phase plane.

gusts. Consequently, a potential scenario is that solution to Problem (20) in not achieved for finite energy signals. In this case the invariant sets can be sought employing the least conservative approach for the class of disturbances with finite energy developed by Hindi and Boyd [28] or, for disturbances of deterministic nature such as discrete gusts, $\mathcal{E}_{as}(\mathbf{P_1}, 1)$ can be numerically found through extensive time simulations.

The application of the methodology presented has therefore predicted the possibility to suppress flutter for the wing section under investigation at the selected flight speed V_{des} while fulfilling the requirement of actuator deflection limit, and a preliminary control law based on the computed values of k, $\boldsymbol{f}(\varepsilon)$, $\boldsymbol{f_0}$ has been built. The final step is the assessment of rate limit fulfillment, which is achieved carrying out time simulations for initial state values in the neighborhood of the origin employing the nonlinear actuator model displayed in Fig. 4. The CL response for both CT and discrete gust encounters at V_{des} with zero initial state is presented in Fig. 12 and 13. It is evident that the AFS controller achieves the design objectives of state stabilization without encountering rate saturation at V_{des} as $|\dot{\beta}|(t) \leq 50$ rad/s for any disturbance input. In case of discrete gust encounters, asymptotic stabilization to the origin is

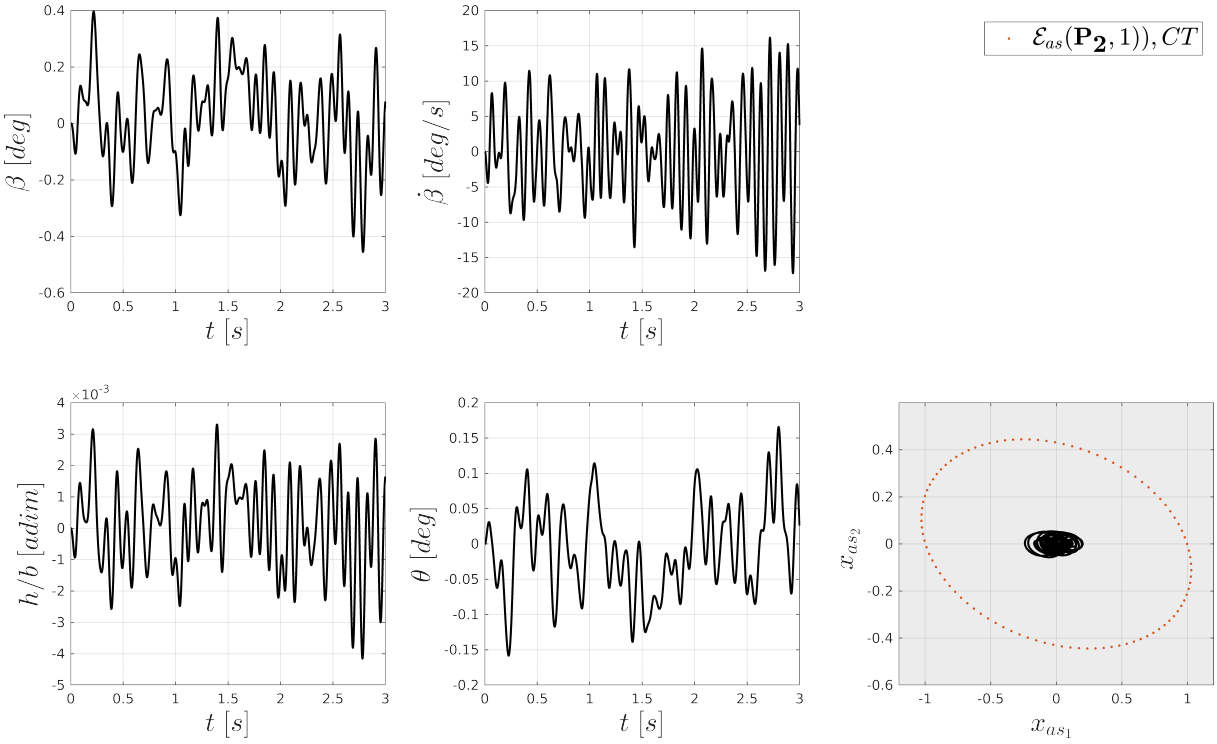

Figure 12: CL Time evolution of the wing section to different CT encounters at V_{des} and projection of state trajectories on anti-stable phase plane.

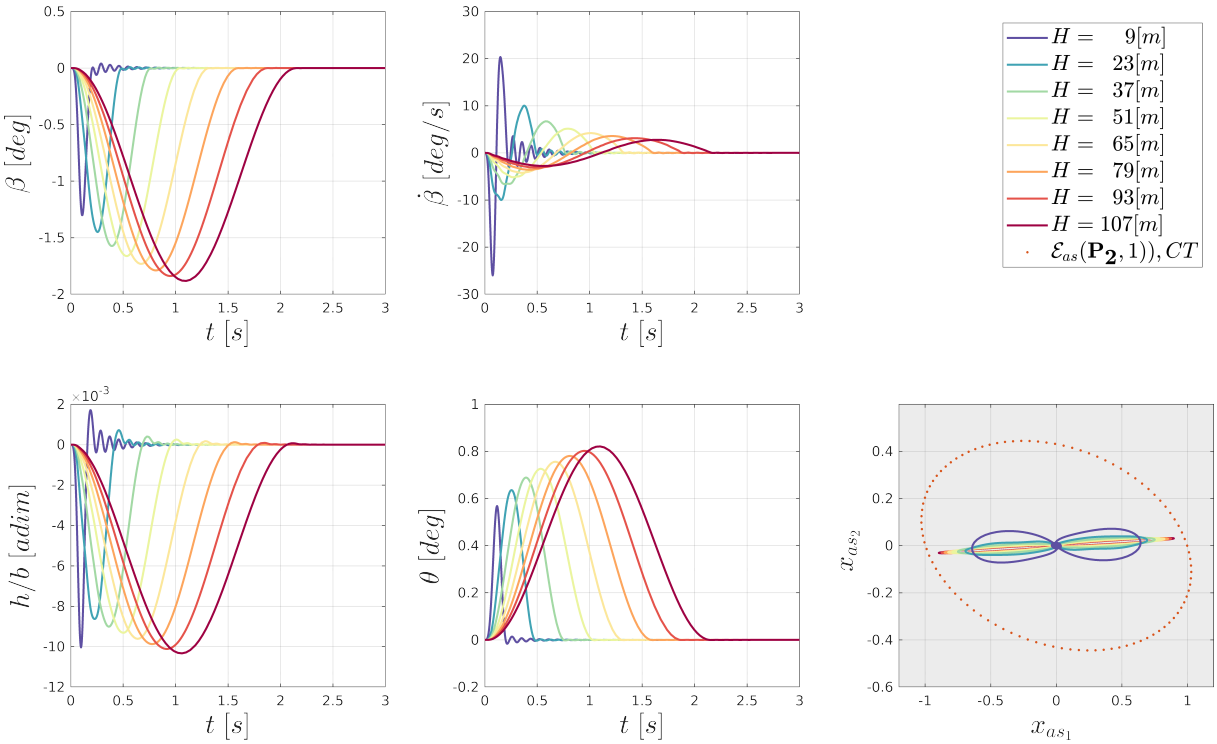

Figure 13: CL Time evolution of the wing section to different discrete gusts encounters at V_{des} and projection of state trajectories on anti-stable phase plane.

achieved, while for CT the trajectories keep bounded in a neighborhood of the origin, different than the previously computed $\mathcal{E}_{as}(\mathbf{P_2}, 1)$ (displayed for comparison purposes), as shown in the bottom-right plot of Fig. 12. Finally, sensitivity studies employing non-zero initial condi-

tions and discrete gust perturbations have been carrying out showing that the system is able to stabilize only a small neighborhood of the origin when rate saturation is also accounted. The so-numerically estimated ROA $\mathcal{E}_{as}^{rate}$ is found to be $\mathcal{E}_{as}^{rate}(\mathbf{P_1}, 1) \subset \mathcal{E}_{as}(\mathbf{P_2}, 1)$, hence significantly smaller compared to the ROA computed when considering only deflection limits. On top of that, the latter estimation relies on time simulations that cannot be employed in case of CT as the problem should be formulated in a stochastic manner. This finding reveals the need to further develop the theoretical background for invariant set analyses and ROA estimation when rate saturation is also accounted, so that a thorough understanding of the CL stability performance can be acquired.

4.2 Example of unfeasible AFS

In this subsection a wing section with different structural properties, an actuator with lower performances, as well as more severe perturbations are considered to provide an example of unfeasible AFS. In particular, the ratio between bending and torsional frequency ω_h/ω_α is taken as $\omega_h/\omega_\alpha = 0.4$, $\beta(t)$ and $\dot{\beta}(t)$ are set to be limited respectively by ± 9 deg and ± 30 deg/s, and a severe turbulence perturbation (the probability of the turbulence intensity being exceeded is selected as 10^{-5} which results in a turbulence intensity $\sigma_w \approx 23$ ft/s at an altitude of 10000 ft [24]) is considered to assess semi-global practical stabilization. The design objectives for the controller are kept as in Subsection 4.1. The selected design speed is $V_{des} = \sqrt{1.2} V_{fl}^{OL} \approx 109.0$ m/s. At this flight point the system presents a pair of complex conjugated unstable poles $p = 0.1568 + i0.6145$ rad/s due to the bending mode instability. The methodology described in Section 3 is applied with $\gamma_{as} = 0.94$ and $\gamma_{ss} = 6$ resulting in a full state control law $\beta_c(t) = \mathrm{sat}(\mathbf{F}\boldsymbol{x_{pl}}(t))$ that ensures semi-global practical stabilization when the system is s.t. deflection limit. Nevertheless, the so-synthesized control law fails in rejecting CT disturbances when rate limit is also accounted, hence resulting in a AFS unfeasible scenario of the 4^{th} kind (see Fig. 5). The response of the wing section for zero initial state due to a severe CT encounter at V_{des} is shown in Fig. 14. As can be seen from the figure, the designed controller cannot stabilize the bending motion $h(t)/b$ and the pitch angle $\theta(t)$ due to the rate saturation of the aileron actuator which degrades the CL system performance. A new aeroelastic plant configuration would be required with the target of reaching the design speed V_{des}.

An application of the methodology in a parametric manner varying the assumed value of β_{max} reveals that design condition 2, namely $\mathcal{S} \subset \mathcal{X}^{des}$ cannot be achieved for values of $\beta_{max} < 8$ deg (see Fig 15), namely any value of β_{max} lower than 8 deg would result in a AFS unfeasible scenario of the 1^{st} kind (see Fig. 5). Fixing a design speed, similar parameter studies can be carried out varying any structural or geometrical parameter to generate an aeroelastic plant with guaranteed $\mathcal{S} \subset \mathcal{X}^{des}$ fulfillment. This is the approach depicted in Fig. 1. Nevertheless, the variation of $\mathcal{C}_{as}$ for different values of $\dot{\beta}_{max}$, which would be interested to address AFS unfeasible scenarios of the 4^{th} kind, cannot be assessed employing the methodology presented here. Since these scenarios are the most frequent, the theory needs to be developed further.

5 CONCLUSIONS AND FUTURE WORK

In this paper, a systematic methodology to assess AFS feasibility for a generic multiple-input LTI aeroelastic plant at the outset of the design phase with actuator deflection and rate limits is presented. The methodology features a systematic workflow to discriminate the attainability of AFS at a given design point based on the concept of semi-global practical stabilization. In viable scenarios, the methodology provides a saturated full-state feedback law with minimum disturbance rejection capabilities as well as no closed-loop performance degradation caused by

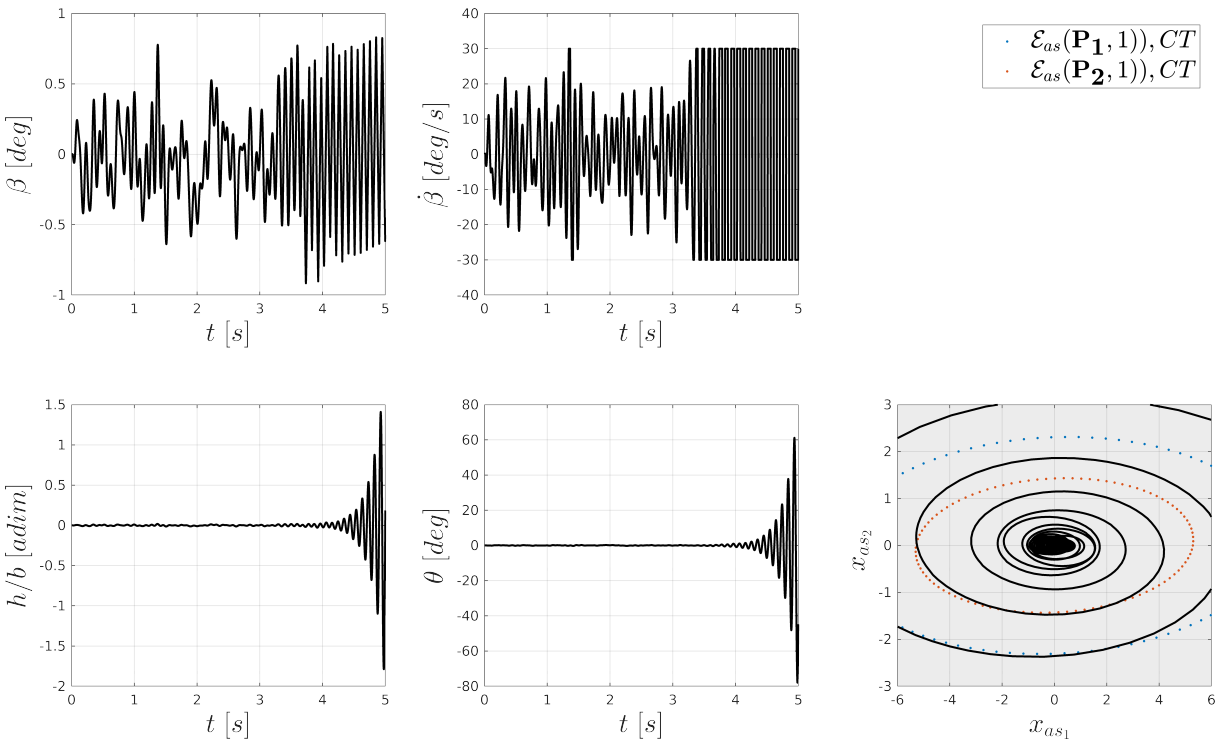

Figure 14: CL time evolution of the wing section to different CT encounters at V_{des} and projection of state trajectories on anti-stable phase plane.

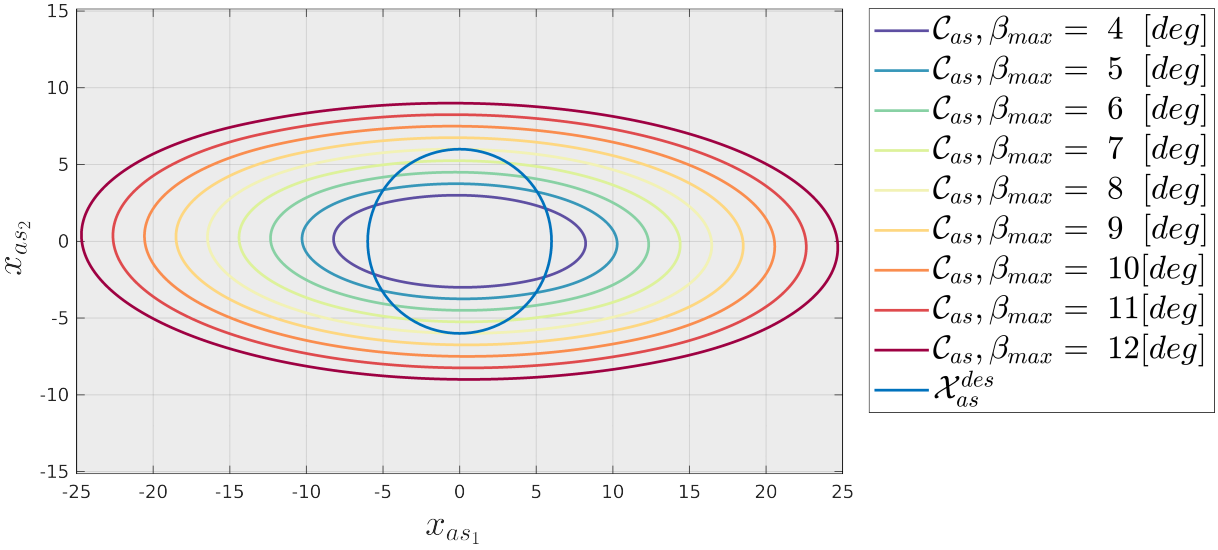

Figure 15: Projection of null controllable region on anti-stable phase plane for different values of deflection limit.

actuator saturation. In simulation case studies, the so-designed preliminary AFS controller has shown to be effective in suppressing flutter instabilities. The preliminary designed controller must be understood as an ideal scenario where accurate state measurements are available. In a later stage of the AFS control design process, the current state-feedback control has to be extended to observer-based output-feedback control, because the aerodynamic states cannot be directly measured, and for measurable states, their sensor signals may be corrupted by noise or affected by aeroelastic modes. The impact of other factors such as sensor noise, sensor errors, time delays, and structure errors has also to be addressed.

The methodology can be used in an iterative fashion to ensure AFS feasibility over a range of

operating conditions. In this regard, stabilization can be achieved through a gain-scheduled controller based on airspeed and altitude.To formally model this control problem, a linear parameter varying (LPV) control design must be employed to give a set of LPV set-invariant conditions that ensure no performance degradation due to actuator saturation and external disturbances. The method is currently under investigation and will be released in the near future. Finally, as discussed in both Subsection 4.1 and 4.2, actuator rate limits might be more constraining than deflection limits, hence degrading the achieved semi-global practical stability performance. To acquire a deeper understanding of the limitations imposed by rate saturation, the environment defined by the last two bullet points of Section 1, where rate saturation plays an active role in the design of the AFS controller, has to be developed.

FUNDING

This work was performed in the context of LuFo project INTELWI and funded by the Bundesministerium für Wirtschaft und Klimaschutz.

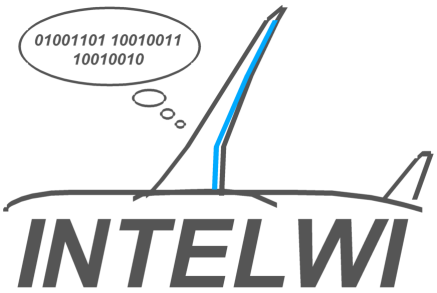

6 REFERENCES

[1] Livne, E. (2003). Future of Airplane Aeroelasticity. *Journal of Aircraft*, 40(6), 1066–1092. doi:10.2514/2.7218.

[2] Bisplinghoff, A. H., R. L. and Halfman, R. L. (1955). *Aeroelasticity*. Reading, MA: Addison-Wesley.

[3] Livne, E. (1999). Integrated Aeroservoelastic Optimization: Status and Direction. *Journal of Aircraft*, 36(1), 122–145. doi:10.2514/2.2419.

[4] Lin, Z. and Lin, Z. (1999). *Low gain feedback*, vol. 240. Springer.

[5] Lin, Z. (1997). Semi-global stabilization of linear systems with position and rate limited actuators. In *Proceedings of the 1997 American Control Conference (Cat. No.97CH36041)*, vol. 2. pp. 1297–1301 vol.2. doi:10.1109/ACC.1997.609745.

[6] TANG, W., WANG, Y., GU, J., et al. (2020). LPV modeling and controller design for body freedom flutter suppression subject to actuator saturation. *Chinese Journal of Aeronautics*, 33(10), 2679–2693. ISSN 1000-9361. doi:https://doi.org/10.1016/j.cja.2020.05.027.

[7] Hu, T., Lin, Z., and Qiu, L. (2001). Stabilization of exponentially unstable linear systems with saturating actuators. *IEEE Trans. Autom. Control.*, 46, 973–979.

[8] Hu, T. and Lin, Z. (2001). *Control Systems with Actuator Saturation: Analysis and Design*. USA: Birkhauser Boston, Inc. ISBN 0817642196.

[9] Klimmek, T., Schulze, M., Abu-Zurayk, M., et al. (2019). cpacs-MONA – An independent and in high fidelity based MDO tasks integrated process for the structural and aeroelastic design for aircraft configurations. In *IFASD 2019 - International Forum on Aeroelasticity and Structural Dynamics*.

[10] Roger, K. L. (1977). Airplane math modeling methods for active control design.

[11] Karpel, M. (1982). Design for Active Flutter Suppression and Gust Alleviation Using State-Space Aeroelastic Modeling. *Journal of Aircraft*, 19(3), 221–227. doi:10.2514/3.57379.

[12] Quero, D., Kaiser, C., Vuillemin, P., et al. (2019). A state-space model for loads analysis based on tangential interpolation.

[13] Quero, D., Vuillemin, P., and Poussot-Vassal, C. (2021). A generalized eigenvalue solution to the flutter stability problem with true damping: The p-l method. *Journal of Fluids and Structures*, 103. doi:10.1016/j.jfluidstructs.2021.103266.

[14] Tang, M., Böswald, M., Govers, Y., et al. (2021). Identification and assessment of a nonlinear dynamic actuator model for controlling an experimental flexible wing. *CEAS Aeronautical Journal*, 12. doi:10.1007/s13272-021-00504-y.

[15] Hájek, O. (1991). *Control Theory in the Plane*. Berlin: Springer-Verlag.

[16] J. Macki, A. S. (1982). *Introduction to Optimal Control Theory*. Berlin: Springer-Verlag.

[17] Singh, S. K. and Nagar, S. K. (2002). Stable / unstable system decomposition tools for continuous & discrete systems and its application to model reduction.

[18] Khalil, H. K. (2002). *Nonlinear systems; 3rd ed.* Upper Saddle River, NJ: Prentice-Hall. The book can be consulted by contacting: PH-AID: Wallet, Lionel.

[19] Theodorsen, T. (1949). General theory of aerodynamic instability and the mechanism of flutter. Tech. Rep. TR-496, NACA.

[20] Jones, R. T. (1940). The unsteady lift of a wing of finite aspect ratio.

[21] Jeličić, G., Böswald, M., and Brandt, A. (2021). Improved computation in terms of accuracy and speed of LTI system response with arbitrary input. *Mechanical Systems and Signal Processing*, 150, 107252. ISSN 0888-3270. doi:https://doi.org/10.1016/j.ymssp.2020.107252.

[22] VON KARMAN, T. and SEARS, W. R. (1938). Airfoil Theory for Non-Uniform Motion. *Journal of the Aeronautical Sciences*, 5(10), 379–390. doi:10.2514/8.674.

[23] EASA (2017). Certification specifications for large aeroplanes cs-25.

[24] Hoblit, F. M. (1988). Gust loads on aircraft: Concepts and applications.

[25] Wu, Z. (2018). Modeling of airfoil aeroelastic response to gust and rain coupled loads. *AIP Advances*, 8(11), 115026. doi:10.1063/1.5064459.

[26] Edwards, J. W., Ashley, H., and Breakwell, J. V. (1979). Unsteady aerodynamic modeling for arbitrary motions. *AIAA Journal*, 17(4), 365–374. doi:10.2514/3.7348.

[27] Waszak, M. (1998). Modeling the benchmark active control technology wind-tunnel model for active control design applications.

[28] Hindi, H. and Boyd, S. (1998). Analysis of linear systems with saturation using convex optimization. In *Proceedings of the 37th IEEE Conference on Decision and Control (Cat. No.98CH36171)*, vol. 1. pp. 903–908 vol.1. doi:10.1109/CDC.1998.760808.

COPYRIGHT STATEMENT